Investigations of Reservoir Response to Net Negative CO_2 Reinjection using Full Scale Geothermal Reservoir Models

Abigail Swanepoel[1], Muhammad Raihannur[2], Aryan Karan [1], Michael Gravatt [1], Ryan Tonkin [1,] John O'Sullivan [1], Jérémy Riffault [2], and Michael O'Sullivan [1]

[1]Department of Engineering Science and Biomedical Engineering, University of Auckland, 70 Symonds Street, Auckland, New Zealand (Aotearoa)

[2] Geothermal Institute, 70 Symonds Street, Auckland, New Zealand (Aotearoa)

michael.gravatt@auckland.ac.nz

Keywords: *Geothermal, Reservoir modelling, Numerical modelling, CO_2 reinjection, Net zero, Net negative, Waiwera*

ABSTRACT

Geothermal power production is a renewable form of base-load electricity generation. However, it is not an emissions-free process due to non-condensable gases, such as CO_2 found naturally underground that are mixed into the working fluid. With the global push toward more sustainable operation of infrastructure, good management of the CO_2 emissions in geothermal fields has financial, environmental and cultural benefits. One strategy is to inject 100% of the CO_2 produced by the system in what is known as a net zero reinjection scheme. Furthermore, additional CO_2 can be captured from other processes, such as the burning of biomass fuels in hybrid biomass geothermal power generation plants and added to the existing reinjection streams. This is known as a net negative injection scheme.

However, successful sequestration of CO_2 using these methods requires knowledge of how the reinjection strategies affect the system, particularly relative to its natural state. Directly monitoring all CO_2 emissions across the surface of the geothermal system in sufficient detail is impractical. Estimation of these emissions can be done using numerical modelling, where short-term CO_2 accumulation under the clay cap is used as a proxy for CO_2 emissions in the long term. This project used a synthetic model to perform numerical simulation of a no CO_2 reinjection production scenario, a 100% CO_2 reinjection scenario and a 110% CO_2 reinjection scenario using Waiwera, an open-source geothermal flow simulator.

In the case with no CO_2 reinjection we observe a steady decline in production CO_2. The two cases where we reinject CO_2 (100% and 110%), we show production CO_2 is consistent with the base case for the first 3.5 years, then we observe a steady increase over the duration of the simulation. In the base case, CO_2 leaves the model either through production or the surface. When injection of CO_2 occurs, the CO_2 is replenished in the production zone of the reservoir from reinjection and the up flow resulting in elevated CO_2 production and more CO_2 going through the alteration in time.

1. INTRODUCTION

There is increasing global interest in carbon sequestration as it is an important factor in mitigating climate change (Snæbjörnsdóttir et al., 2020). The push to reduce greenhouse gas (GHG) emissions comes from the 2015 Paris Agreement, which saw 196 parties commit to limiting global warming to a maximum of +2 °C (UNFCCC, 2016). The UK Department of Energy and Climate Change, 2012 estimates that Carbon Capture and Storage (CCS) will need to constitute 20% of the global reductions in emissions needed to meet the 2050 target.

The New Zealand government has set several domestic targets for the country to meet the objective of the Paris Agreement. The current target is to have net zero GHG emissions by 2050, except for biogenic methane (Ministry for the Environment, 2023). A key part of this aim is decarbonising Aotearoa's electricity generation. In New Zealand, geothermal energy is a favourable form of renewable base load electricity and accounts for between 18 and 19% of electricity generation (Ministry of Business, Innovation and Employment, 2023). However, the escape of non-condensable gases (NCGs) mixed in with the geothermal working fluid means that geothermal energy production is not an emission-free process. In fact, of all the renewable energy sources utilised in Aotearoa, geothermal power stations have the highest operational emissions intensity (McLean et al., 2020). Therefore, careful consideration of how to reduce the emissions of geothermal power plants is critical.

Sections 1.1 and 1.2 further outline the context of the work in this paper, and Section 1.3 discusses the research aims and assumptions in this work. The synthetic full-scale geothermal reservoir model is outlined in Section 2, with preparation of the production histories for three injection strategies discussed in Section 3. Analysis of the results of the simulations can be found in Section 4.

1.1 Numerical Modelling of CO_2

While methods of measuring CO_2 emissions at the surface level exist, making measurements at the level of detail required for serviceable surface output calculations is impractical (O'Sullivan et al., 2021). Furthermore, measurements cannot be made retrospectively. Computer modelling, therefore, plays an important role in determining the CO_2 emissions over a geothermal project's lifetime and the system's behaviour beyond that.

Numerical modelling of NCG-water reinjection by Kaya and Zarrouk (2017) suggests that reservoir recharge and steam production improve under well-designed reinjection systems. The models also suggest that reinjection of NCGs can be an environmentally friendly way to dispose of NCGs. Raihannur (2024) simulated twenty years of production under a CO_2 reinjection strategy where the CO_2 concentration of the injectate was held constant at 1%, along with a base case of 0% CO_2 reinjection. However, numerical modelling by Gravatt et al. (2021) demonstrated that the measured production emissions can vary greatly from the modelled change in surface emissions. This work also highlighted the limitations of the numerical modelling approach. Although numerical modelling is a well-established method of portraying system behaviour, surface features are difficult to represent in these models.

Furthermore, model calibration typically focuses on matching the behaviour of the wells, making calibration of these surface

features a lower priority. However, these features are of interest for accurately measuring CO_2 emissions at the ground surface, as outlined by Bertani and Thain (2002). The CO_2 that accumulates under the clay cap in the short term can be used as a proxy for surface emissions, assuming that the CO_2 will eventually be emitted from the reservoir through the surface features. Therefore, the accuracy of this numerical modelling approach has a notable impact on how the effectiveness of a CCS strategy is measured.

1.2 CO_2 Management in Aotearoa New Zealand

Implementation of CCS has begun in New Zealand in several trials. Ngāwhā Geothermal Power Station is a binary power plant situated on the only high enthalpy geothermal field used for power generation outside of the Taupo Volcanic Zone (TVZ) (ThinkGeoEnergy, 2023). It is also unique in that it has almost no surface features through which natural degassing can occur due to the caprock on the field (Ngāwhā Generation, 2023). This means that the geothermal fluid at Ngāwhā has unusually high levels of operational CO_{2e} at approximately 8.3% (McLean et al., 2020). The high carbon emissions saw the power station using almost 30% of its revenue to pay its carbon tax and receiving recommendations to shut down before Ngāwhā began their Carbon Zero Project. The project was budgeted to cost $6 million but was delivered at a few hundred thousand dollars because the transition to 100% CO_2 reinjection impacted operation far less than expected (ThinkGeoEnergy, 2023). The success of Ngāwhā's Carbon Zero Project demonstrates the technical feasibility and economic viability of such a scheme as a part of Aotearoa New Zealand's CCS journey.

However, unlike Ngāwhā, approximately 105 of New Zealand's geothermal fields are low temperature systems and are underutilised due to the high costs associated with their operation (Cheptum, 2023). The key to utilising these low enthalpy geothermal systems may lie in utilising them in combination with biomass (Titus et al., 2022). The process of combining bioenergy sources with carbon capture and storage strategies (BECCS) is a technology that currently lacks widespread use due to the high operational cost of transporting the captured carbon to reinjection sites and the high capital expenditure involved in developing the reinjection sites themselves (Titus et al., 2022).

Geothermal plants have established reinjection protocols for geothermal fluid, which can be adapted to incorporate CO_2 injection with little disruption. It is proposed that burning biomass to provide additional heating for the geothermal fluid could solve both problems (Titus et al., 2023). Hybrid geothermal-BECCS plants have the dual advantage of increasing the feasibility of low enthalpy geothermal fields and the carbon capture stages of BECCS without sacrificing financial viability (Titus et al., 2023). Primary industries in New Zealand produce a consistent 10 million cubic meters of woody biomass yearly (BioPacific Partners et al., 2020). This feedstock absorbs atmospheric CO_2 as it grows, which would be captured and sequestered underground in a geothermal-BECCS hybrid plant. The proposed cycle, therefore, becomes not just net carbon neutral but net carbon negative. The reinjection of CO_2 produced by geothermal plants back into their reservoirs has been successful thus far, but the economic viability and technological feasibility of net negative schemes have only begun to be studied in recent years. Globally, initiatives attempting net negative carbon sequestration in fields where mineral trapping can occur have shown success (Clark et al., 2020). However, the geological formations in Aotearoa New Zealand are less favourable to this type of sequestration than those in Australia (Al Kalbani et al., 2023). The effect of dissolving additional biogenic CO_2 in the reinjection fluid on the resulting reservoir behaviour has not been thoroughly investigated and is included as one of the injection strategies investigated in this paper.

1.3 Research Objectives

This paper focuses on modelling CO_2 sequestration. It aims to investigate how a simple geothermal system responds to CO_2 reinjection by comparing the reservoir response for different injection strategies using numerical simulation.

Several factors of interest are analysed in the results. Firstly, the CO_2 flow across the bottom of the clay cap is analysed as a proxy for CO_2 emissions, as discussed in Section 1.1. The CO_2 flow rate in the production wells is also of interest since, in a real geothermal system, this can influence the efficiency of the geothermal power plant. Similarly, it is important to analyse what effect the CO_2 injection has on the pressure of the system since these play a crucial role in the productivity of a geothermal system.

1.3.1 Modelling Assumptions

When CO_2 is injected, underground mineralisation can occur under favourable conditions. However, geochemical reactions in the reservoir are not considered in this work. Furthermore, the model does not account for any above-ground factors that would affect the operation of a real geothermal power system. For example, the impact of different CO_2 concentrations in the production steam on the maintenance of power generation equipment has been ignored. Additionally, the CO_2 injection schemes do not consider the increased likelihood of slug flow, the onset of which can make it difficult to control production rates due to pressure fluctuations and subsequent vibrations that can damage equipment (Zarrouk & Purnanto, 2015). Instead, the model assumes that CO_2-water mixtures travel successfully into and out of the wells. We also assume that CO_2 capture in the geothermal power plant is 100% efficient, such that no CO_2 is lost from when it leaves the ground to when it re-enters and that the CO_2 can be reinjected almost immediately, with no delay in matching the produced and injected rates.

2. SYNTHETIC MODEL

The numerical model used to investigate the effect of CO_2 reinjection in geothermal reservoirs is an existing model developed by Raihannur (2024). The digital conceptual model shown in Figure 1 was created by GNS Science to reflect the typical characteristics of existing convective geothermal fields in New Zealand (Renaud et al., 2022). The clay cap is represented by the magenta region in Figure 1.

Waiwera is used to run production scenarios for this synthetic system. The parallelisation capability of Waiwera allows for relatively simple interfacing with the New Zealand eScience Infrastructure (NeSI) high-performance computing facilities, specifically with NeSI's supercomputer. This allows for a significant speed-up in computational time.

The numerical grid for this model has 31023 blocks over an area of 13 km × 15 km with 32 layers reaching a depth of 2750 m. Grid refinements exist around the area of interest, i.e., around the wells, faults and clay cap, as is visible in Figure 2. The largest blocks measure 1000 m^2, with the most refined measuring 200 m^2.

Atmospheric conditions are specified at the top surface of the model, with the pressure at 1 bar and temperature at 12.3 °C. A 10% infiltration rate with 1000 m of annual rainfall is also applied. The modelled area is sufficiently larger than the synthetic reservoir to assume that there are no significant

flows through the sides of the model. Therefore, no-flow boundary conditions are enforced at the sides of the model.

As this is a synthetic system, the reservoir engineering data typically used to calibrate a reservoir model does not exist. Instead, the model was calibrated to produce a typical convective geothermal system with temperatures ranging from 190-210 °C below the clay cap. To achieve this, a background heat flux of 100 MW/m^2 is uniformly applied to the base of the model. The hot upflow of water and CO_2 is specified on the bottom boundary of the model to represent convective mass flow from below the numerical model. The location and size of the upflow are shown in Figure 3. The upflow totalled to 28 kg/s of water at an enthalpy of 1500 kJ/kg. The CO_2 flow totalled to 0.70 kg/s, which is 2.5% of the inflow and is in line with CO_2 levels found in some systems in New Zealand. This calibration results in the distinctive convective plume evident in the cross-section of Well 3, shown in Figure 4 (a), with the accompanying downhole temperature plot in Figure 4 (b).

This model has four injection wells, five production wells, and two monitoring wells. In Figure 2, Wells 5, 6, 7 and 8, shown in blue, are the injection wells. Wells 2, 3, 9, 10 and 11, shown in red, are the production wells. Wells 1 and 4, shown in black, are monitor wells.

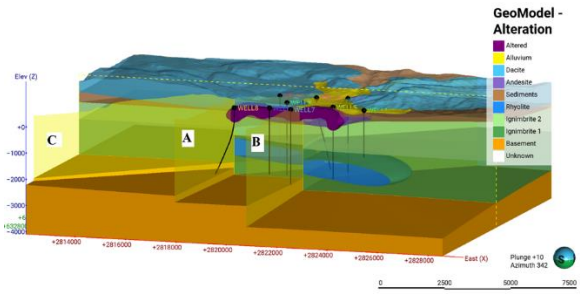

Figure 1: 3D representation of the lithologies around faults A, B and C (Raihannur, 2024).

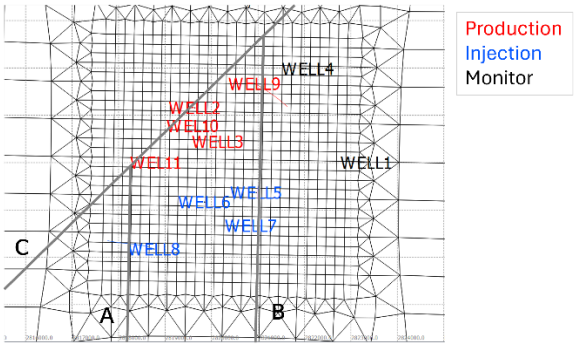

Figure 2: 2D image showing grid refinements around the wells and faults.

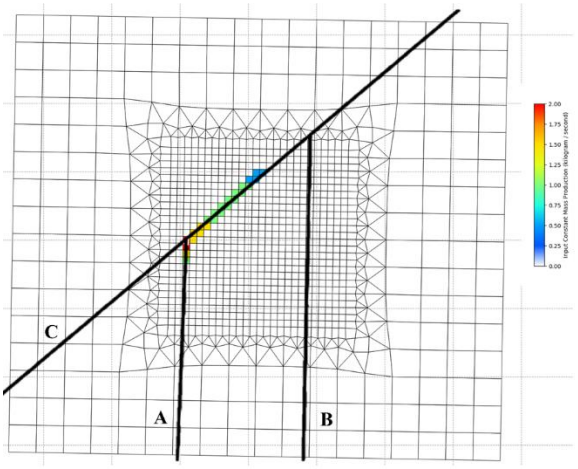

Figure 3: 2D figure showing the 'generator blocks' specifying the mass inflow along the faults (Raihannur, 2024).

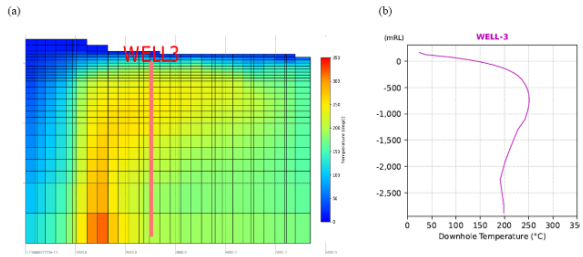

Figure 4: Cross-section of the upflow near Well 3 (a) and its downhole temperature plot (b).

3. METHODS

This work investigates the response of a synthetic geothermal system to different amounts of CO_2 injection over a twenty-year production period. Three production scenarios are considered. The first scenario is a 0% CO_2 injection case, i.e., no CO_2 is reinjected back into the reservoir. The production and injection rates for this scenario are shown in Figure 5. This scenario acts as a baseline against which the other CO_2 reinjection strategies are compared. The second production scenario injects 100% of the CO_2 drawn up by the production wells back into the reservoir. The CO_2 injected, therefore, matches the CO_2 produced. The third production scenario is an injection strategy that injects 110% of the CO_2 drawn up by the production wells back into the reservoir. This is designed to simulate a net negative scenario like those discussed in Section 1.2.

3.1 Production History Setup

Each production scenario is run from 2017 to 2037, a period of twenty years. Synthetic production and injection rates were generated for each well to target 40 MW of power generation and 75% reinjection (Raihannur, 2024). These are shown in Figure 5. For the first year of the simulation, Well 6 is the only operating injection well, and Well 3 is the only operating production well, as shown in Figure 5 (a) and (b), respectively. With the exception of Well 10, the other wells then begin operation in 2018, with the flow rates in the production wells ramping up a few months before the injection wells follow suit. Operations cause a reduction in pressure, which in turn causes a decline in production rates over time, visible in Figure 5 (b). This correlates with the decline in the injection mass flow between 2017 and 2024, as seen in Figure 5 (a). In this model, Well 10 is a make-up well that comes online in 2024. The increase in production rate

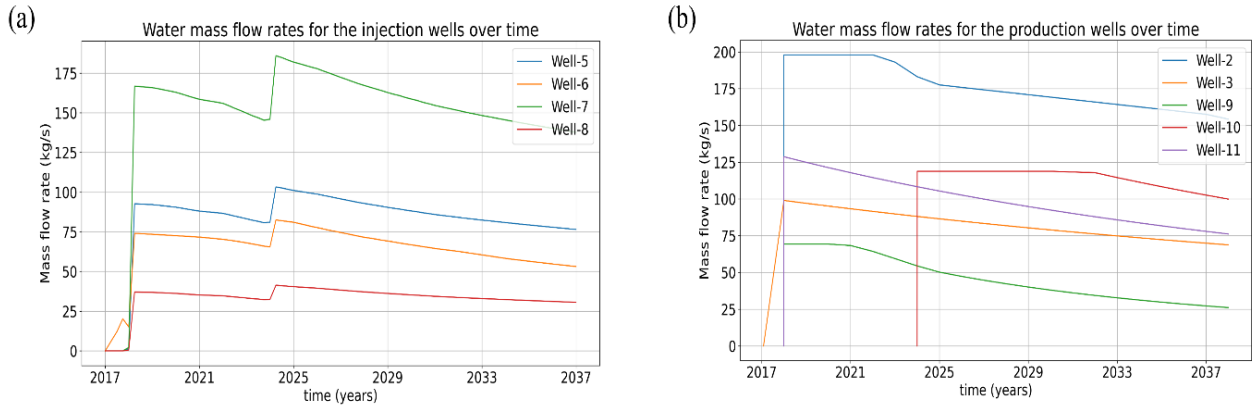

Figure 5: Water mass flow rates for the injection wells (a) and production wells (b) over the twenty-year simulation.

provided by Well 10 corresponds to the increase in injection mass flow rate, as seen in Figure 5 (a).

The water flow rate for each injection well remains constant for all three scenarios. This means any CO_2 injected into the well is added to the existing water stream. It is assumed that this CO_2 is fully dissolved in the injectate by the time it enters the reservoir. This model, therefore, does not account for the behaviour of the water-CO_2 mixture in the wells.

3.1.1 Convergence Algorithm for Reinjection Rate

For the 100% and 110% reinjection cases, changing the amount of CO_2 injected into the geothermal system will alter the reservoir dynamics. Therefore, the amount of CO_2 produced is likely to change, which will, in turn, alter the amount of CO_2 that needs to be injected to maintain the same proportion of CO_2 in the injectate. Hence, the rate of CO_2 injection cannot be determined directly from the baseline scenario. Because there is no current capability to adaptively adjust the CO_2 injection mass flow rate according to the amount of CO_2 produced by the production wells during the simulation, an iterative approach is necessary. This iterative process is shown in Figure 6.

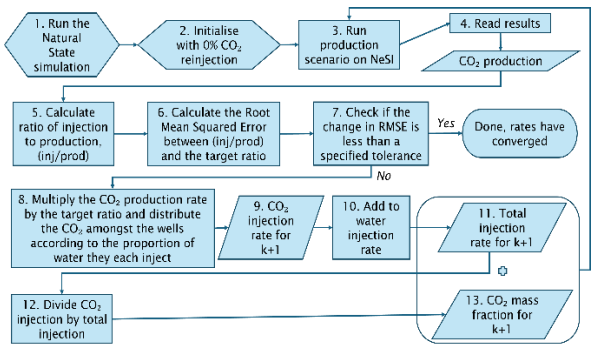

Figure 6: Iterative process for calculating the CO_2 injection mass flow rate.

Steps 1-2 in Figure 6 involve the set-up of the natural state of the system and the initial CO_2 injection mass flow rate for iteration $k = 0$. The key inputs to Waiwera are the total injection mass flow rate, and the fraction of this mass flow rate that is CO_2. For the 0th iteration, the total mass flow rates are those in Figure 5, and the CO_2 mass fraction is 0% across all the wells over the twenty-year simulation period.

In Steps 3-4, the production scenario is run on NeSI and the CO_2 production mass flow rates are read from the results.

In Steps 5-6 in Figure 6, ratios of the CO_2 injection mass flow rates vs these CO_2 production mass flow rates yield r in

$$RMSE^k = \sqrt{\frac{\sum_{i=1}^{n} (r_i^k - \tilde{t})^2}{n}} \quad (1)$$

where RMSE is the Root Mean Squared Error at iteration k, i is the timestep, n is the total number of timesteps, and t is the target proportion. The target proportions used for the injection strategies are 1.0 for the 100% CO_2 reinjection case and 1.1 for the 110% reinjection case. The iteration terminates if

$$\left| RMSE^k - RMSE^{k-1} \right| \geq tol \quad (2)$$

where *tol* is the acceptance tolerance for the convergence of the RMSE. The tolerance used in Step 7 was 1×10^{-6}.

If the RMSE has not converged, then the CO_2 production rate is used in Step 8 in

$$inj_{w,i}^{k+1} = prod_i^k \times t \times prop_{w,i}$$
$$\forall\, i = 1,2,\ldots,n\,,\ w \in W_{inj} \quad (3)$$

where $inj_{w,i}^{k+1}$ is the CO_2 injection mass flow rate for the next iteration for well w, $prod_i^k$ is the production mass flow rate at time i and iteration k, and $prop_{w,i}$ is the proportion of the total mass flow rate injected by well w at time i for all the injection wells, W_{inj}. These proportions are calculated using the water mass flow rates (see Figure 5). The CO_2 is distributed across the injection wells according to their flow proportion.

Steps 9-13 use

$$tot_{w,i}^{k+1} = inj_{w,i}^{k+1} + wat_{w,i}$$
$$\forall i = 1,2,\ldots,n\,,\ w \in W_{inj} \quad (4)$$

and

$$mf_{w,i}^{k+1} = \frac{inj_{w,i}^{k+1}}{tot_{w,i}^{k+1}} \forall i = 1,2,\ldots,n\,,\ w \in W_{inj} \quad (5)$$

to calculate the inputs into production run $k+1$, where $tot_{w,i}^{k+1}$ is the total injection mass flow rate for well w at time i, $wat_{w,i}$ is the corresponding water mass flow rate, and $mf_{w,i}^{k+1}$ is the updated CO_2 mass fraction.

For each production scenario, the change in RMSE between successive iterations fell below the specified tolerance of 1.0×10^{-6} after five iterations. Figure 7 shows the convergence of the RMSE to approximately 0.15 in the 100% CO_2 reinjection case. Figure 8 shows that using the solution with this RMSE results in a negligible difference between injected and produced rates of CO_2, with a total difference over the twenty years of 2.3×10^{-5} kg/s.

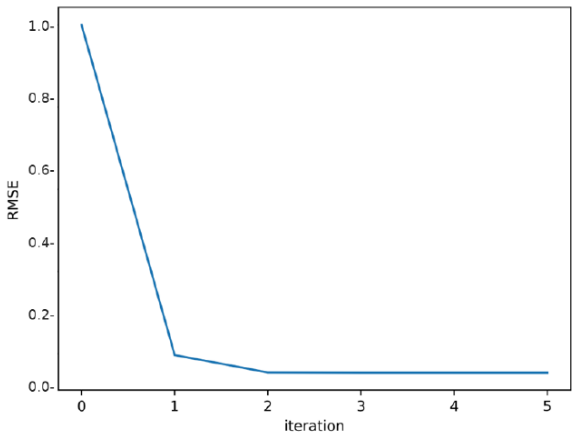

Figure 7: Plot showing the convergence of the RMSE across iterations.

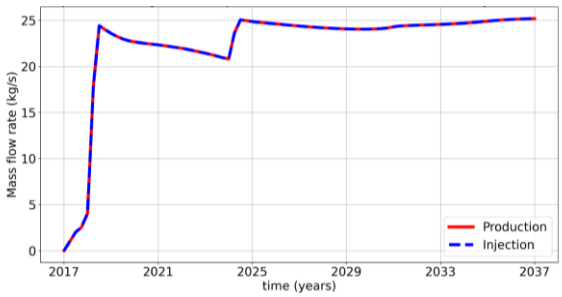

Figure 8: Convergence of CO_2 injection rates to CO_2 production rates for the 100% CO_2 reinjection case.

3.2 Processing of Simulation Results

In this work, we analyse the CO_2 emissions from the geothermal system. This includes the CO_2 production rate in the wells and the flow rate of CO_2 from surface features. These factors influence the profitability and sustainability of the geothermal field in the long term. The production CO_2 rate is readily obtained from either data or the modelling results, but estimating the CO_2 flow rate from surface features has several challenges because there is no way to model the surface emissions exactly, as is discussed in Section 1.1. In this work, a water and CO_2 equation of state is used to represent the CO_2 in the system. However, this also means that the atmosphere is modelled as pure CO_2. This is because there is currently no EOS that accounts for water, air and CO_2 in Waiwera. This treatment of the atmosphere means that the modelled CO_2 fluxes at the ground surface, represented by 1 in Figure 9, are not reflective of reality. This is because any pressure decrease in the reservoir that would cause a drawdown of air instead causes a drawdown of CO_2 in the numerical model.

The clay cap, shown at 2 in Figure 9, is a suitable analogue for the surface, under the assumption that the CO_2 that accumulates under the clay cap in the short term will eventually be emitted from the reservoir through the surface features. Therefore, in this work, we use the CO_2 mass flow across the bottom of the clay cap as a proxy for CO_2 flow at the surface when considering the effect of CO_2 injection on the background emissions of the reservoir.

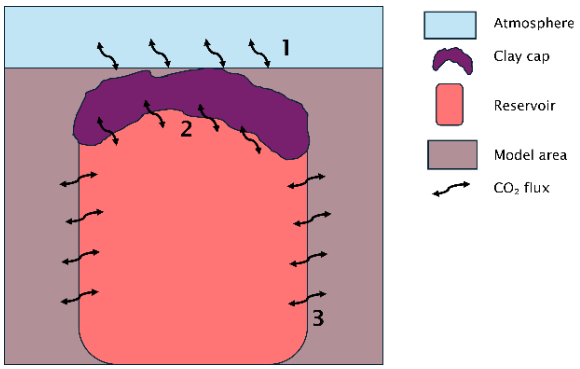

Figure 9: Boundaries for measuring CO_2 flux.

4. RESULTS

The CO_2 mass flow rate across the bottom of the clay cap is analysed and compared across the three production scenarios, with CO_2 flow up across the bottom of the clay cap characterised as positive and CO_2 flow down as negative. The base case scenario is analysed in Section 4.1. The effect of 100% CO_2 reinjection (net zero) and 110% CO_2 reinjection (net negative) on net CO_2 mass flow rate through the clay cap, CO_2 mass fraction in the production wells and pressure support in the reservoir are compared to the base case in Section 4.2.

4.1 Base Case

The initial CO_2 mass flow rate through the base of the clay cap in the base case scenario is shown in Figure 10, with the locations of the wells and faults shown. While the CO_2 flow is distributed across the clay cap, there is more accumulation around the centre. There is a slightly higher CO_2 flow along Fault B and around Well 2. This is due to the CO_2 flowing up with the primary upflow and accumulating at the shallowest point of the clay cap. Furthermore, there is some downward flow of CO_2 on the western side of the clay cap, indicated by the pale blue colouring. This results in a net CO_2 mass flow rate of approximately 0.40 kg/s through the bottom of the clay cap, which is the starting net CO_2 mass flow rate for each production scenario.

Figure 11 plots the net CO_2 flux through the clay cap for the base case over the twenty-year production period. There are two noticeable decreases in the net CO_2 mass flow rate for the base case scenario. These correspond with additional wells coming online, first in 2018 and then the make-up Well 10 in 2024, as discussed in Section 3.1. Producing from a geothermal system decreases the pressure in the reservoir over time.

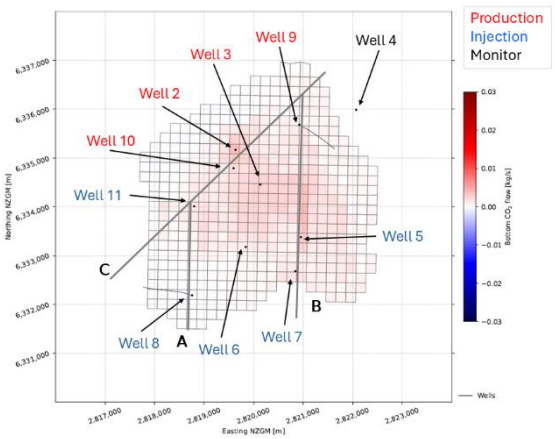

Figure 10: CO_2 flow across the base of the clay cap at the start of the production scenario.

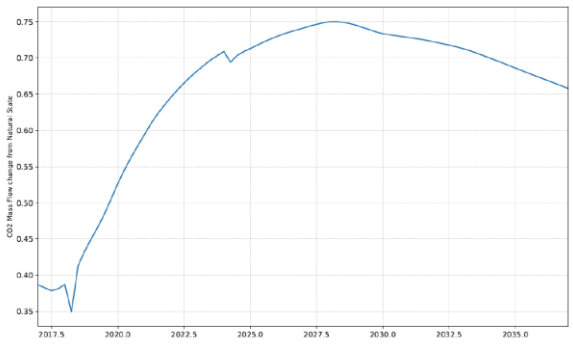

Figure 11: Net CO_2 mass flow at the bottom of the clay cap for the base case scenario over time.

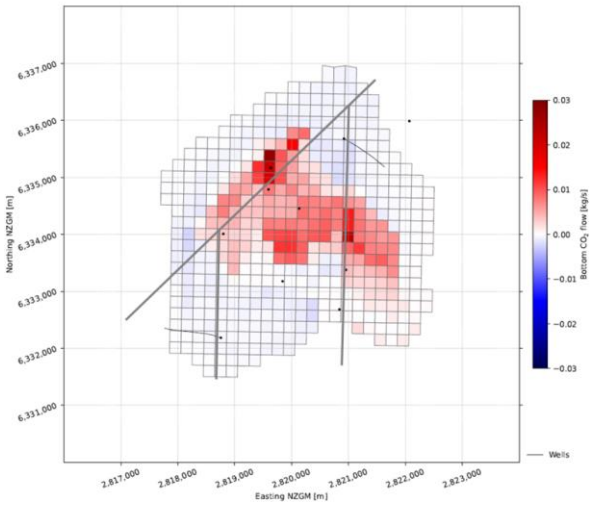

Figure 12: Base case distribution of CO_2 mass flow at the bottom of the clay cap in 2027.

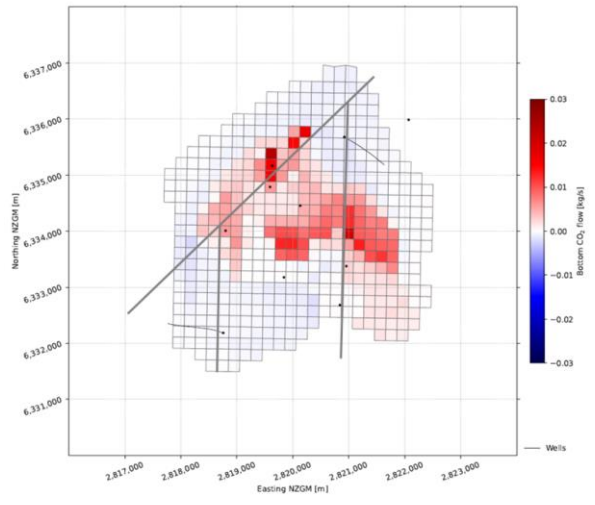

Figure 13: Base case distribution of CO_2 mass flow at the bottom of the clay cap in 2037.

This induces boiling and causes CO_2 to come out of solution, making it more mobile. This increased mobility corresponds with an increase in the mass flow rate of CO_2, shown by the overall increasing trend in CO_2 mass flow rate up through the clay cap for the first ten years of production. The distribution of the CO_2 flow in 2027 is shown in Figure 12. The upflow is more obvious in this figure than in Figure 10, with far more CO_2 flow through the shallower parts of the clay cap in the centre. The maximum net CO_2 mass flow rate up across the clay cap is approximately 0.75 kg/s, which is 0.45 kg/s higher than the initial rate. However, as production continues without any reinjection of CO_2, the system undergoes degassing, with the net CO_2 mass flow up across the clay cap declining to a rate of approximately 0.65 kg/s in the final state shown in Figure 13.

Overall, the base case scenario demonstrates the impact of production and injection rates on reservoir pressure and the subsequent change in the net mass flow rate of CO_2 based on changes to its mobility. The base case scenario also shows the tendency of CO_2 to follow the upflow stream and accumulate in shallow parts of the clay cap.

4.2 100% CO_2 and 110% Reinjection Cases

The 100% CO_2 reinjection simulation is run from the same natural state as the base case scenario, with the CO_2 injection specified following the procedure outlined in Section 3.1. As outlined in Section 3.1, the water mass flow rates are kept the same across all three scenarios, with the injected CO_2 being added into the existing injection streams. This means the total injection mass flow rate for the net zero CO_2 reinjection case is greater than that of the base case, and higher pressures are maintained in the reservoir. Therefore, the addition of Well 10 in 2024 has less of an effect than for the base case scenario.

Figure 14 shows that the net CO_2 mass flow rate increases consistently to 4.8 kg/s at the end of the twenty-year simulation. Comparing Figure 14 with Figure 11 indicates that CO_2 flux through the clay cap increases when CO_2 is injected back into the geothermal system. This suggests that for this system, CO_2 reinjection will likely result in elevated background CO_2 emissions from the geothermal system during production, despite reinjection activities. However, this increase is much smaller than the CO_2 that would have been emitted when CO_2 was not returned to the reservoir. Additionally, Figure 15 indicates that the CO_2 mass fraction in the production fluid increases due to CO_2 reinjection. At the end of the production period, the average CO_2 mass fraction in the production fluid is 1.37% in the base case and 2.09% in the 100% CO_2 reinjection scenario. The increase in CO_2 is attributed to shallow feeds in some reinjection wells causing increased CO_2 concentration in the shallow reservoir, as shown in Figures 16 and 17.

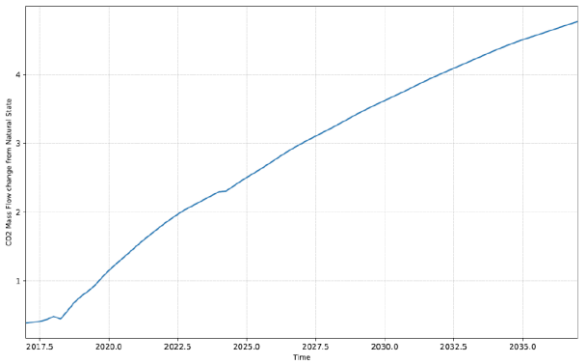

Figure 14: Net CO_2 mass flow at the bottom of the clay cap for the net zero case over time.

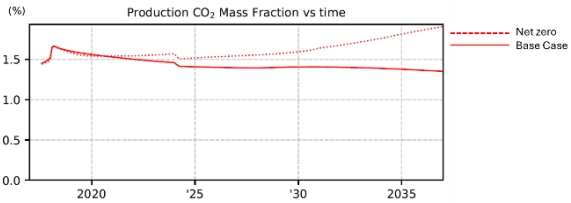

Figure 15: Comparison of production CO_2 mass fraction between the base and net zero case.

The net negative (110%) reinjection case shows similar results. Specifically, the net CO_2 mass flow rate in Figure 18 across the bottom of the clay cap for the 110% CO_2 reinjection scenario shows a similar trend to the 100% CO_2 reinjection case in Figure 14. However, the final net CO_2 mass flow through the clay cap is higher, at 5.8 kg/s (compared to 4.8 kg/s). Similarly, Figure 19 shows that there is higher production CO_2 mass fraction in the production fluid for the 110% reinjection case, which reaches a maximum of 2.26% at the end of production (compared to 2.09%).

Both CO_2 reinjection cases reduced pressure decline in the reservoir. This is shown in the comparison of feed pressure for Well 2, the largest producing well in this system, given in Figure 20. Here, feed pressures are approximately 10 bar higher when CO_2 is reinjected. This indicates that CO_2 reinjection could have a positive impact on reservoir pressure decline.

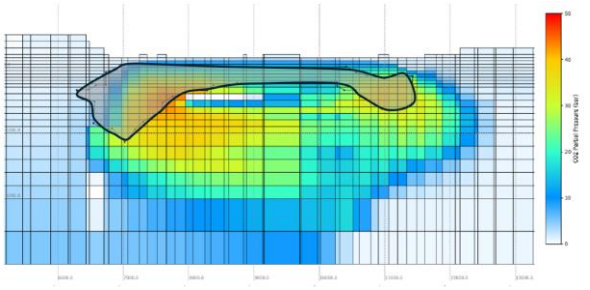

Figure 16: Base case distribution of CO_2 partial pressure in the reservoir in 2037. The approximate location of the clay cap is shown in grey.

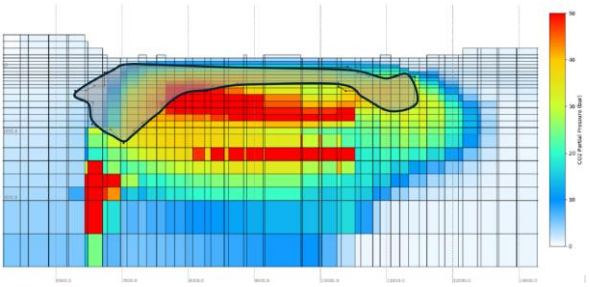

Figure 17: Net zero case distribution of CO_2 partial pressure in the reservoir in 2037. The approximate location of the clay cap is shown in grey.

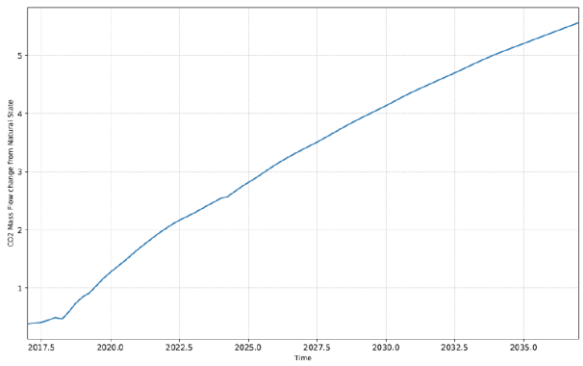

Figure 18: Net CO_2 mass flow at the bottom of the clay cap for the net negative case over time.

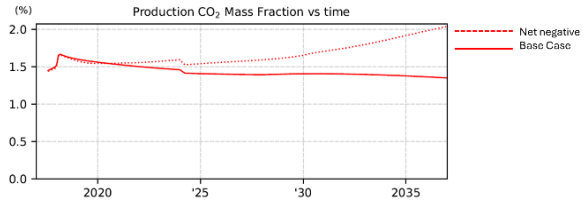

Figure 19: Comparison of production CO_2 mass fractions between the base and net negative case.

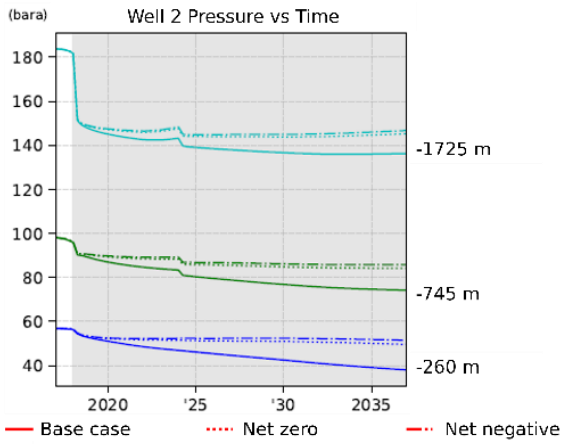

Figure 20: Comparison of pressure vs time in the three feed zones of Well 2 across the three cases.

5. CONCLUSIONS

This work investigated the impact of CO_2 reinjection on a synthetic geothermal system. We considered three cases, no CO_2 reinjection, net-zero CO_2 reinjection and net-negative CO_2 reinjection. For each case, we investigate how the net CO_2 mass flow rate through the clay cap and CO_2 mass fraction in the production wells changes due to CO_2 reinjection.

In the case with no CO_2 reinjection, we observe a steady decline in production CO_2. In the two cases where we reinject CO_2 (100% and 110%), we show production CO_2 is consistent with the base case for the first 3.5 years. Then, we observe a steady increase over the duration of the simulation. In the base case, CO_2 leaves the model either through production or the surface. When injection of CO_2 occurs, the CO_2 is replenished in the production zone of the reservoir from reinjection and the upflow, resulting in elevated CO_2 production and increased CO_2 flow through the alteration as time progresses.

This work considers a synthetic geothermal system. A similar approach could be taken with real geothermal systems to understand how CO_2 reinjection affects their operation and to optimise CO_2 reinjection strategies.

REFERENCES

Al Kalbani, M., Serati, M., Hofmann, H., & Bore, T. (2023). A comprehensive review of enhanced in-situ CO2 mineralisation in Australia and New Zealand. International Journal of Coal Geology, 276(104316). https://doi.org/10.1016/j.coal.2023.104316

Bertani, R., & Thain, I. (2002). Geothermal power generating plant CO2 emission survey. IGA news, 49, 1–3.

BioPacific Partners, FP Innovations, Nawtika, & Russell Burton & Associates. (2020). Wood Fibre Futures investment in the use of commercial forest biomass to move New Zealand towards carbon-zero Stage One Report (tech. rep.). https://www.mpi.govt.nz/dmsdocument/41824/direct

Cheptum, I. (2023). Preliminary assessment of low enthalpy Ohinewai geothermal system (tech. rep.). Waikato Regional Council. Retrieved October 9, 2024, from https://www.waikatoregion.govt.nz/assets/WRC/WRC-2019/TR201308.pdf

Clark, D. E., Oelkers, E. H., Gunnarsson, I., Sigfússon, B., Snæbjörnsdóttir, S. Ó., Aradóttir, E. S., & Gíslason, S. R. (2020). CarbFix2: CO2 and H2S mineralization during 3.5 years of continuous injection into basaltic rocks at more than 250 °C. Geochimica et Cosmochimica Acta, 279, 45–66. https://doi.org/https://doi.org/10.1016/j.gca.2020.03.039

Croucher, A., O'Sullivan, M., O'Sullivan, J., Yeh, A., Burnell, J., & Kissling, W. (2020). Waiwera: A parallel open-source geothermal flow simulator. *Computers & Geosciences*, p. 141, 104529. https://doi.org/https://doi.org/10.1016/j.cageo.2020.104529

Department of Energy and Climate Change. (2012). CCS Roadmap Supporting Deployment of Carbon Capture and Storage in the UK. https://assets.publishing.service.gov.uk/media/5a758e07ed915d506ee7fbab/4899-the-ccs-roadmap.pdf

Gravatt, M., O'Sullivan, J. P., Popineau, J., & O'Sullivan, M. J. (2021). Numerical Modelling for Carbon Accounting from Geothermal Power Plants, Proceedings 43rd New Zealand Geothermal Workshop, Wellington, New Zealand.

Kaya, E., & Zarrouk, S. J. (2017). Reinjection of Greenhouse Gases into Geothermal Reservoirs. International Journal of Greenhouse Gas Control, 67, 111–129.

McLean, K., Richardson, I., Quinao, J., Clark, T., & Owens, L. (2020). Greenhouse Gas Emissions from New Zealand Geothermal Power Generation and Industrial Direct Use, Proceedings 42nd New Zealand Geothermal Workshop, Waitangi, New Zealand.

Ministry of Business, Innovation and Employment. (2023). Electricity statistics - Fuel type (GWh). https://www.mbie.govt.nz/assets/Data-Files/Energy/nz-energy-quarterly-and-energy-in-nz/electricity-sept.xlsx

Ministry for the Environment. (2023). Greenhouse gas emissions targets and reporting. Retrieved April 16, 2024, from https://environment.govt.n/what-government-is-doing/areas-of-work/climate-change/emissions-reductions/emissions-reduction-targets/greenhouse-gas-emissions-targets-and-reporting/

Ngāwhā Generation. (2023). Our path to net carbon zero by 2025. Retrieved October 9, 2024, from https://ngawhageneration.co.nz/tell-me-about/news/our-path-to-net-carbon-zero-by-2025

O'Sullivan, M., Gravatt, M., Popineau, J., O'Sullivan, J., Mannington, W., & McDowell, J. (2021). Carbon dioxide emissions from geothermal power plants. *Renewable Energy, p. 175*, 990–1000. https://doi.org/https://doi.org/10.1016/j.renene.2021.05.021

Raihannur, M. A. (2024). Using a Numerical Model to Investigate the Effect of Geothermal Production and Reinjection on the Natural CO2 Flux from a Geothermal System [Master's thesis, Department of Engineering Science and Biomedical Engineering, University of Auckland].

Renaud, T., Popineau, J., Riffault, J., O'Sullivan, J., Gravatt, M., Yeh, A., Croucher, A., & O'Sullivan, M. (2022). Practical workflow for training in geothermal reservoir modelling. https://doi.org/10.1016/j.envsoft.2023.105666

Snæbjörnsdóttir, S., Sigfússon, B., Marieni, C., Goldberg, D., Gislason, S. R., & Oelkers, E. H. (2020). Carbon dioxide storage through mineral carbonation. https://doi.org/10.1038/s43017-019-0011-8

ThinkGeoEnergy. (2023). Ngawha becomes New Zealand's first zero-carbon geothermal power station. Retrieved April 20, 2024, from https://www.thinkgeoenergy.com/ngawha-becomes-new-zealands-first-zero-carbon-geothermal-power-station/

Titus, K., Archer, R., Peer, R., & Dempsey, D. (2022). Carbon Negative Geothermal: Financial Analysis for Combined Geothermal, Bioenergy and Carbon Dioxide Removal. Proceeding 44th New Zealand Geothermal Workshop, Auckland, New Zealand.

Titus, K., Dempsey, D., & Peer, R. (2023). Carbon negative geothermal: Theoretical efficiency and sequestration potential of geothermal-BECCS energy cycles. *International Journal of Greenhouse Gas Control, p. 122*, 103813. https://doi.org/10.1016/j.ijggc.2022.103813

UNFCCC. (2016). The Paris Agreement. United Nations Climate Change. https://unfccc.int/ process-and-meetings/the-paris-agreement

Zarrouk, S. J., & Purnanto, M. H. (2015). Geothermal steam-water separators: Design overview. Geothermics, 53, 236–254. https://doi.org/https://doi.org/10.1016/j.geothermics.2014. 05.009